Local atomic structure of semiconductor alloys using pair distribution functions

Jean S. Chung* and M. F. Thorpe
Department of Physics and Astronomy, Michigan State University, East Lansing, Michigan 48824
and Center for Fundamental Materials Research, Michigan State University, East Lansing, Michigan 48824
(Received 5 August 1996)

We have developed a method of calculating the pair distribution function of binary semiconductor crystals and pseudobinary alloys with the zinc-blende structures. The pair distribution function is essentially the density-density correlation function and reveals the local structure directly. We have used a simple model using a harmonic potential with bond-stretching and bond-bending forces. The temperature dependence has been incorporated quantum mechanically. Results of this method are presented for both crystals (InAs and GaAs) and alloys ($Ga_{1-x}In_xAs$). These results can be directly compared with x-ray and neutron-diffraction experiments. [S0163-1829(97)06004-9]

I. INTRODUCTION

Semiconductor alloys have been studied extensively due to their importance in applications. These materials have received much attention because physical properties, such as the band gap, mobility, and lattice parameter, can be continuously controlled.[1] Having such continuous controls is of importance in applications such as electronic devices or optical devices. For example, the energy gap of a pseudobinary compound $Ga_{1-x}Al_xAs$ can be varied between 1.4 and 2.2 eV by varying the composition x, and the wavelength of the solid-state laser made from this material can be tuned accordingly.

Unlike pure crystals, the difference in the bond lengths associated with different chemical species in alloys induces internal strain. The structural characterization of alloys dates back to the work of Vegard,[2] who found that the lattice constants of some alloys change linearly with the concentration of the constituents. A simplistic explanation of this phenomenon is the virtual-crystal approximation,[3] in which all the atoms are located on an ideal lattice with the lattice constant given by the compositional average of the constituents. Therefore, this approximation completely neglects the local deformations, which would be expected to occur. In tetrahedrally coordinated semiconductor compounds, deformation also occurs in the bond angles. A better understanding of Vegard's law in random alloys was achieved recently and the conditions under which Vegard's law is expected to hold were given.[4] These studies used a harmonic potential, which accounts for the bond-stretching and the bond-bending forces. It has been shown that Vegard's law is strictly obeyed when the force constants for bond-stretching and the bond-bending forces are the same for the end members from which the alloy is made, and are independent of the composition. In semiconductor alloys, these simplifications were exploited in a series of recent papers.[5–8] Most semiconductor alloys made from III-V and II-VI elements follow Vegard's law very closely.[6]

The experimental structural characterization of alloys has been accomplished mainly using Bragg x-ray diffraction, and also using Bragg neutron diffraction. These experiments measure the structural quantities that are correlated over *long* distances, such as the lattice constant. Recently, extended x-ray absorption fine structure (XAFS) experiments have been used to study semiconductor alloys.[9] Such experiments investigate the *short*-range order, such as the near-neighbor spacings.

However, the diffuse background in diffraction experiments has not drawn much attention because it is more difficult to obtain and hard to analyze. Nonetheless, the diffuse background exists in all experimental data on alloys due to the local displacements. This information can be analyzed using the pair distribution function (PDF). PDF analysis has been used mainly in the characterization of atomic arrangements in amorphous materials such as noncrystalline alloys or liquids.[10–12] Although it has long been known that the PDF method is well suited for analyzing crystalline as well as amorphous materials, it has only recently been applied to study the local structure of disordered crystalline materials.[13] Because the real-space resolution is inversely proportional to the highest momentum data, it is essential to have *high-momentum* scattering data to study local structures. High momentum scattering data have become available with the advent of synchrotron x-ray sources and spallation neutron sources. These high-momentum scattering data not only give information about local structures from the diffusive background but also allow accurate data normalization. Since it has now become rather routine to access the high-momentum scattering data, PDF analysis is becoming a good candidate for characterizing semiconductor alloys.

There are several attractive features to using PDF analysis. On the one hand, it covers a wide range of pair distances. Therefore, it can be used to study local structural characteristics such as nearest-neighbor distances and intermediate-range structures such as clustering. On the other hand, it gives a complete description of the structure in that not only the average distance between a pair but the *width* of the length distribution can also be obtained, with good accuracy. Furthermore, this method is not subject to any arbitrary fitting parameters and the result of a theoretical calculation can be directly compared with the experimental data.

In this paper, we present a method of calculating the PDF of binary semiconductor crystals in the zinc-blende structure, AC, and the associated pseudobinary alloys, $A_{1-x}B_xC$. We

also discuss the advantages and limitations of using the PDF analysis in investigating local structures. To account for the local strain, we use a simple valence-bond model,[6] which has been successful in describing the local strain in semiconductor alloys. Since experimental data are always subject to thermal broadening, thermal averaging should be taken into account also. This is done in this paper by using the proper Bose factors and also by employing the Debye-Waller theorem. We limit ourselves in our discussion of the PDF of semiconductor alloys to the zinc-blende structure in the form of *random solid solutions*. In particular, we focus on $Ga_{1-x}In_xAs$ as an important example. But our method can be easily modified to any crystals and crystalline alloys; with or without local clustering present.

The reason for choosing $Ga_{1-x}In_xAs$ is that it is one of the largest bond-length mismatched alloys among III-V and II-VI compounds. Therefore, the effect of bond-length disorder will be most pronounced. Also it is one of the standard systems and has been studied quite extensively.[6,9] One of the experimental advantages is that the two end members, GaAs and InAs, are completely miscible and form a random solid solution at *all* concentrations.

II. MODEL

To account for the forces between atoms tetrahedrally coupled by the valence bonding in zinc-blende structures, we adopt the Kirkwood model.[15] The potential energy in this model is given by

$$V=\sum_{\langle i,j\rangle}\frac{\alpha_{ij}}{2}(L_{ij}-L_{ij}^0)^2+L_e^2\sum_{\langle ij,il\rangle}\frac{\beta_{ijl}}{8}(\cos\theta_{ijl}-\cos\theta^0)^2. \tag{1}$$

Here, the first term describes the energy due to the bond-stretching force with the force constant α_{ij} between atoms i and j. L_{ij} and L_{ij}^0 are the actual and natural (unstrained) bond lengths between atoms i and j, respectively. The second term in (1) is due to the bond-bending force with the force constant β_{ijl} between the bonds ij and il. θ_{ijl} and θ^0 are the actual and natural (109.5°) angle between the bonds ij and il. L_e is the nearest-neighbor distance as given by the virtual crystal approximation. L_e is inserted in the second term to make β_{ijl} have the same dimension as α_{ij}. The angular brackets under the summations denote counting each configuration only once to exclude double counting. The potential (1) has been used extensively in discussing the elastic strain in semiconductor alloys.[5–8] The harmonic approximation can be applied because we expect *small* positional changes in the alloy from the virtual crystal, which is used as a reference. There are two causes for the distortions, the *static* one from the bond-length mismatch and the *dynamic* one from the thermal motion. The change from bond-length mismatch is small since it is less than 10% of the unstrained bond lengths although $Ga_{1-x}In_xAs$ is one of the largest length-mismatched semiconductors. The thermal broadening is also quite small since we are interested in the low-to-room-temperature range. It is therefore reasonable to use a harmonic approximation for the potential due to the displacements.

Let $\mathbf{u}_i$ be the displacement vector of atom i from its perfect crystalline position. Expanding up to linear terms in $\mathbf{u}_i$, we have

$$L_{ij}=L_e+\hat{r}_{ij}\cdot\mathbf{u}_{ij}, \tag{2}$$

where $\hat{r}_{ij}$ is a unit vector in the perfect crystal pointing from atom i to its nearest neighbor j, and $\mathbf{u}_{ij}=\mathbf{u}_j-\mathbf{u}_i$. Then the potential energy (1) can be expanded to have the form[6]

$$V=\sum_{\langle i,j\rangle}\frac{\alpha_{ij}}{2}(L_e-L_{ij}^0+\hat{r}_{ij}\cdot\mathbf{u}_{ij})^2 +L_e^2\sum_{\langle ij,il\rangle}\frac{\beta_{ijl}}{8}\left[\hat{r}_{ij}\cdot\mathbf{u}_{il}+\hat{r}_{il}\cdot\mathbf{u}_{ij}+\frac{1}{3}(\hat{r}_{ij}\cdot\mathbf{u}_{ij}\hat{r}_{il}\cdot\mathbf{u}_{il})\right]^2. \tag{3}$$

We[5–8] have preferred to use the Kirkwood model Eq. (3) rather than the more popular Keating model[16] because of the cleaner separation of length and angular displacements. Since the nearest-neighbor central force alone is not enough to stabilize the zinc-blende structure, this model is one of the simplest force models for the zinc-blende structure. This model (3) is not good enough to produce very exact phonon dispersion relations. However, it has been proved to be accurate enough to describe the local structure quantitatively.[6] It also provides a clear picture for the important microscopic forces. Therefore, the model is a good starting point for our purpose and may be refined later as needed. It appears that this simple model can capture all the essential features in the PDF.

Equation (3) can be recast into a concise matrix form,

$$V=\tfrac{1}{2}\mathbf{u}^\dagger\mathbf{M}\mathbf{u}+\mathbf{u}^\dagger\mathbf{\Phi}+E_0, \tag{4}$$

where $\mathbf{u}=(\mathbf{u}_1,\mathbf{u}_2,\dots)$ is the displacement field vector and $\mathbf{M}$ is a matrix derivable from Eq. (3). The components of the force vector field $\mathbf{\Phi}=(\mathbf{\Phi}_1,\mathbf{\Phi}_2,\dots)$ are defined by

$$\mathbf{\Phi}_i=-\sum_j\alpha_{ij}(L_e-L_{ij}^0)\hat{r}_{ij}, \tag{5}$$

which expresses the internal strain due to the disorder. The length disorder only appears through this vector. This form of the potential (4) is useful in that it gives a simple form to find the relaxed equilibrium positions of strained systems, namely,

$$\mathbf{M}\mathbf{u}=-\mathbf{\Phi}, \tag{6}$$

and also in that the dynamical matrix is defined through the matrix $\mathbf{M}$ as discussed in the next section.

III. DEFINITIONS

Since different definitions are used in the literature,[17] we give the definitions we use in this study. To define the dynamical matrix $\mathbf{D}(\mathbf{k})$, we need to distinguish the Bravais lattice and the basis to which the atom i belongs. Let us divide N atoms into $\mathcal{N}$ Bravais lattice points, each containing p basis atoms $[N=\mathcal{N}p]$. Let $l(l')$ and $\mu(\mu')$ be the Bravais lattice and the basis labels of the atom $i(i')$, respectively. Denoting the position of the atom i as $\mathbf{r}_i$, we use the following definition of the dynamical matrix;

$$\mathbf{D}_{\mu a,\mu' a'}(\mathbf{k})=(M_\mu M_{\mu'})^{-1/2}\sum_{l'} M_{ia,i'a'}e^{-i\mathbf{k}\cdot[\mathbf{r}_i-\mathbf{r}_{i'}]}. \quad (7)$$

Here, a and a' denote three Cartesian coordinates, and hence the dynamical matrix is a $3p\times 3p$ matrix.

Since different nomenclature has been used for the PDF, we hereby give the definition.[14] For the sake of simplicity, we begin with an arrangement of N identical atoms.[10–13] Then, the atomic density function $p(\mathbf{r})$ is given by

$$p(\mathbf{r})=\sum_{\mathbf{r}_i}\delta(\mathbf{r}-\mathbf{r}_i), \quad (8)$$

and the density-density correlation function $C(r)$ can be written as

$$C(\mathbf{r})=\frac{1}{N}\left\langle\int p(\mathbf{r}'+\mathbf{r})p(\mathbf{r}')d\mathbf{r}'\right\rangle=\frac{1}{N}\sum_{\mathbf{r}_i}\sum_{\mathbf{r}_j}\langle\delta(\mathbf{r}-\mathbf{r}_{ij})\rangle$$
$$=\rho(\mathbf{r})+\delta(\mathbf{r}), \quad (9)$$

where $\mathbf{r}_{ij}=\mathbf{r}_j-\mathbf{r}_i$ is a vector from atom i to j and $\langle\rangle$ denotes the statistical average that implies *both* configurational and thermal averages. The correlation function $C(\mathbf{r})$ describes the probability per unit volume of finding an atom at position $\mathbf{r}$ from a chosen atom at the origin. This probability density is further averaged by taking each atom in turn as the origin. The δ function $\delta(\mathbf{r})$ is the probability of finding itself and appears as a constant background in the momentum space of experiments. The function $\rho(\mathbf{r})$ defines the PDF. Defining $\rho_{ij}(\mathbf{r})\equiv\langle\delta(\mathbf{r}-\mathbf{r}_{ij})\rangle$, the PDF can be rewritten as

$$\rho(\mathbf{r})=\frac{1}{N}\sum_{i,j}{}'\rho_{ij}(\mathbf{r}), \quad (10)$$

where the prime in the summation means that $i=j$ is excluded.

In this study, the major interest lies in macroscopically *isotropic* materials, such as pure randomly oriented crystallites or random solid solutions. In such materials, $\rho(\mathbf{r})$ depends only on the magnitude r. It is convenient to define the radial distribution function (RDF) as $J(r)=4\pi r^2\rho(r)$. Then the probability should be interpreted as per unit length rather than per unit volume. The average number of atoms in a shell with radius r and thickness dr is given by $J(r)dr$.

However, the RDF tends to obscure the correlations between atoms as r gets larger because it grows rapidly. Hence, it is customary to define the reduced RDF as

$$G(r)=4\pi r[\rho(r)-\rho_0]=\frac{1}{r}[J(r)-4\pi r^2\rho_0], \quad (11)$$

where ρ_0 is the average *number* density of the material. Since the average density is subtracted, $G(r)$ oscillates around zero and shows the correlations more clearly than does the RDF. Usually, it is this function to which the experimental data are transformed through the relation

$$G(r)=\frac{2}{\pi}\int_0^\infty F(q)\sin qr\,dq. \quad (12)$$

Here q is the magnitude of the scattering vector and $F(q)$ is the reduced scattering intensity defined by

$$F(q)\equiv q\left[\frac{I(q)}{Nf^2}-1\right], \quad (13)$$

where $f(q)$ is the atomic form factor and $I(q)$ is the experimentally measured scattering intensity given by the square of the scattering amplitude,

$$I(q)=\left|\sum_i^N f(q)e^{i\mathbf{q}\cdot\mathbf{r}_i}\right|^2. \quad (14)$$

In the next section, the Kirkwood model of the previous section is utilized to calculate the PDF and results are given mainly in the form of the reduced RDF to be directly compared with experiments.

In case of multicomponent systems,[10–13] the definition of the PDF is generalized to

$$\rho(\mathbf{r})=\frac{1}{N}\sum_{\mathbf{r}_i}\sum_{\mathbf{r}_j}w_{ij}\rho_{ij}(\mathbf{r}). \quad (15)$$

Here, w_{ij} is given by $f_i\underline{f_j/f}$, where f_i is the scattering strength of the atom i and $\overline{f}$ denotes the arithmetic mean of f_i's in the sample. f_i is the scattering factor in x-ray scattering, and the scattering length in neutron scattering. Equation (15) is exact for neutron diffraction, where the scattering is from the nucleus which may be considered as a point. For x-ray scattering Eq. (15) is only an approximation as the f_i are due to the electron density associated with each atom, which in reality have different $\mathbf{q}$ dependence. Nevertheless we will use this approximation here so that the f_i are proportional to the atomic charges Z_i.

IV. CALCULATION OF PDF

In this section we evaluate the PDF of crystalline systems in the zinc-blende structure. The system may be either a pure binary semiconductor such as GaAs and InAs, or a pseudobinary alloy such as $Ga_{1-x}In_xAs$. We first rewrite $\rho_{ij}(r)$ as

$$\rho_{ij}(r)=\frac{1}{2\pi}\int dq e^{-iqr}\langle e^{iqr_{ij}}\rangle. \quad (16)$$

This function would be a δ function located at r_{ij} if all the atoms were stationary in a perfect crystal. However, this δ function is broadened by the *thermal motions* since the atoms move about the equilibrium positions even at zero temperature. Moreover, it is further broadened by the *internal strains* due to the bond-length mismatch in the case of alloys.

For the thermal motions, the Debye-Waller theorem can be applied to the harmonic approximation of Sec. II. As shown in Appendix A, this leads to a *Gaussian* peak for $\rho_{ij}(r)$ centered at r_{ij} with width σ_{ij} given by

$$\sigma_{ij}=\langle[\mathbf{u}_{ij}\cdot\hat{r}_{ij}]^2\rangle^{1/2}. \quad (17)$$

Accordingly, the total PDF consists of a series of Gaussians from each pair in the system with weight w_{ij}.

To proceed further, we make use of the quantum-mechanical representation of the displacement. Let us divide N atoms into $\mathcal{N}$ Bravais lattice points, each containing p basis atoms as before. Let μ (ν) be the basis label of atoms i (j) in a unit cell. Rewriting $\mathbf{u}_{ij}$ in terms of phonon operators, it can be shown that

$$\sigma_{ij}^2=\frac{2\hbar}{N}\sum_{\mathbf{k},s}\frac{1}{\omega_s(\mathbf{k})}\left(\langle n_{\mathbf{k},s}\rangle+\frac{1}{2}\right)\left[\frac{1}{2}\left\{\frac{|e_\mu(\mathbf{k},s)\cdot\hat{r}_{ij}|^2}{M_\mu}+\frac{|e_\nu(\mathbf{k},s)\cdot\hat{r}_{ij}|^2}{M_\nu}\right\}-\frac{|e_\mu(\mathbf{k},s)\cdot\hat{r}_{ij}||e_\nu(-\mathbf{k},s)\cdot\hat{r}_{ij}|e^{i\mathbf{k}\cdot\mathbf{r}_{ij}}}{\sqrt{M_\mu M_\nu}}\right], \tag{18}$$

where $\omega_s(\mathbf{k})$ is the eigenvalue of the dynamical matrix (7) with the wave vector $\mathbf{k}$ in branch s, $n_{\mathbf{k},s}$ is the number operator in that mode, and $e_\mu(\mathbf{k},s)$ is the corresponding eigenvector associated with the basis μ and mass M_μ. In the summation, $\mathbf{k}$ runs from 1 to $\mathcal{N}$ and s runs from 1 to $3p$. Now, the problem of finding the effect of *thermal* broadening is reduced to solving the eigenvalue problem of the dynamical matrix. Solving the eigenvalue problem analytically for general $\mathbf{k}$ has to rely on numerical methods.

Below, we distinguish between the pure and disordered systems. In the former, the only reason for line broadening is the thermal motion. In the latter, there are two reasons, the thermal motion and the internal strains.

A. Pure system

Consider a pure binary semiconductor crystal, AC, with A atoms in one sublattice and C in the other. There is only one source of peak broadening, the *thermal* motion, which is characterized by the σ_{ij} in Eq. (18). For a pure crystal, α_{ij} assumes the same value α for all bonds and we assume that β_{ijl} also takes the same value β for all angles. These parameters can be determined independently from standard experimental data.[6] Since $p=2$ in the zinc-blende structure, the dynamical matrix is a 6×6 matrix. It can be calculated analytically in a closed form for general $\mathbf{k}$:[8]

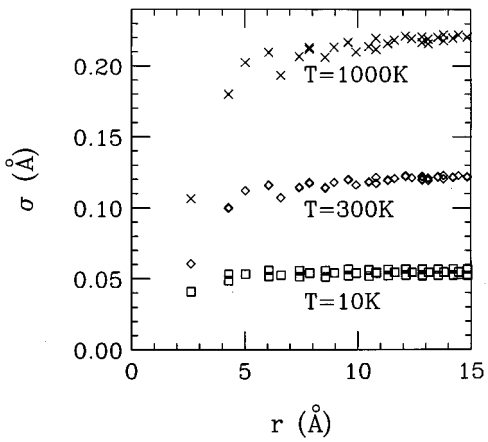

FIG. 1. The width σ for a pure InAs crystal as a function of the distance from the origin r at different temperatures ($\times$, at 1000 K; $\diamond$, at 300 K; and $\square$, at 10 K). The leftmost symbol corresponds to the nearest neighbor. At certain distances, where two types of neighbors (e.g., In-In and As-As) occur, symbols may overlap.

$$D_{\mathbf{k}}=\alpha\begin{bmatrix}\frac{4}{3}\mathbf{1} & -\tau_{-\mathbf{k}}\\ -\tau_{\mathbf{k}} & \frac{4}{3}\mathbf{1}\end{bmatrix}+\beta\begin{bmatrix}\frac{4}{3}\mathbf{1}+\frac{1}{4}\nu_{\mathbf{k}}\nu_{-\mathbf{k}} & \tau_{-\mathbf{k}}-\frac{2}{3}\gamma_{-\mathbf{k}}\mathbf{1}\\ \tau_{\mathbf{k}}-\frac{2}{3}\gamma_{\mathbf{k}}\mathbf{1} & \frac{4}{3}\mathbf{1}+\frac{1}{4}\nu_{-\mathbf{k}}\nu_{\mathbf{k}}\end{bmatrix}+\frac{1}{9}\beta\begin{bmatrix}\frac{4}{3}\mathbf{1}+\frac{1}{4}\nu_{-\mathbf{k}}\nu_{\mathbf{k}}+\frac{4}{3}\gamma_{\mathbf{k}}\tau_{-\mathbf{k}}+\frac{4}{3}\gamma_{-\mathbf{k}}\tau_{\mathbf{k}} & \tau_{-\mathbf{k}}-2\gamma_{-\mathbf{k}}\mathbf{1}\\ \tau_{\mathbf{k}}-2\gamma_{\mathbf{k}}\mathbf{1} & \frac{4}{3}\mathbf{1}+\frac{1}{4}\nu_{\mathbf{k}}\nu_{-\mathbf{k}}+\frac{4}{3}\gamma_{-\mathbf{k}}\tau_{\mathbf{k}}+\frac{4}{3}\gamma_{\mathbf{k}}\tau_{-\mathbf{k}}\end{bmatrix}. \tag{19}$$

Here, $\mathbf{1}$ is the 3×3 unit matrix, and the scalar $\gamma_{\mathbf{k}}$ is given by

$$\gamma_{\mathbf{k}}\equiv\sum_{\boldsymbol{\delta}}e^{-i\mathbf{k}\cdot\boldsymbol{\delta}}=4\left[\cos\frac{k_xL_e}{\sqrt{3}}\cos\frac{k_yL_e}{\sqrt{3}}\cos\frac{k_zL_e}{\sqrt{3}}+i\sin\frac{k_xL_e}{\sqrt{3}}\sin\frac{k_yL_e}{\sqrt{3}}\sin\frac{k_zL_e}{\sqrt{3}}\right]. \tag{20}$$

The vector $\nu_{\mathbf{k}}$ and the tensor $\tau_{\mathbf{k}}$ are defined to be $\nu_{\mathbf{k}}=(i\nabla_{\mathbf{k}}/L_e)\gamma_{\mathbf{k}}$, $\tau_{\mathbf{k}}=(i\nabla_{\mathbf{k}}/L_e)(i\nabla_{\mathbf{k}}/L_e)\gamma_{\mathbf{k}}$, respectively. Using Eq. (19) the eigenvalue problem can be solved numerically, and the summation in Eq. (18) can be carried out using Monte Carlo integration over the first Brillouin zone.

There is *no* internal strain for a pure system as discussed in Sec. II. Figure 1 presents the result for the width σ for InAs at different temperatures. We used $\alpha=105.30$ N/m and $\beta=17.28$ N/m for InAs.[6] Note that there is a factor of 3 difference in the values of the force constants used here and previously[6] due to different definitions. The symbols at 2.62 Å depict the width of nearest neighbors, and those at 4.28 Å represent that of the second neighbors, etc. Although the highest temperature 1000 K is not realistic because it is beyond the melting point, still the width σ is much less than the interatomic spacing. It is to be noted that the width for the nearest neighbors does not vary as much as the widths for other neighbors as the temperature is increased. This is because nearest-neighbor pairs are connected by the strong bond-stretching force. All other neighbors are connected by at least one bond-bending force, which is considerably weaker than the bond-stretching force in covalently bonded materials. Therefore, further neighbors connected by bond-bending forces become more sensitive to the thermal agitation, while nearest-neighbor pairs can remain rather rigid. This has an experimental significance; if one wants to improve the experimental resolution by lowering the temperature, it does not help much for the nearest-neighbor peak,

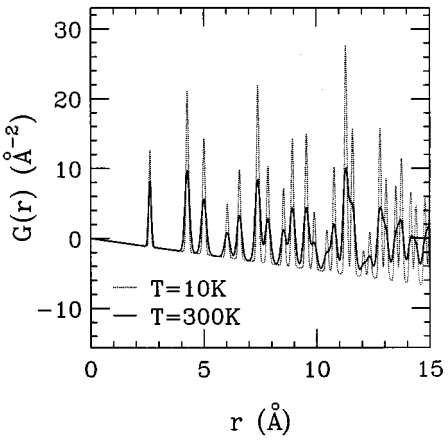

FIG. 2. Temperature dependence of the reduced (x-ray) RDF of a pure InAs crystal is plotted as a function of the distance from the origin r at 10 K (dotted line) and 300 K (solid line). Note that the resolution changes substantially with the temperature.

which turns out to be the most interesting, as it does for the rest of peaks.

In calculating the PDF, the symmetry of the system can be made use of in the summation of Eq. (18). Since the same type of neighbors have the same distance and the same width, PDF peaks of the same type are simply weighted by the number of neighbors of that type in addition to the weighting factor w_{ij}. For example, nearest neighbor by 4, next nearest neighbor by 12, and so on. The reduced RDF $G(r)$ of InAs at 10 K and 300 K are depicted in Fig. 2. The curve at 10 K shows much sharper peaks as expected. As the temperature is raised, however, peak widths are increased and hence peak heights are decreased substantially due to the effect of the thermal broadening.

In Fig. 3, the reduced RDF at 300 K is compared with an x-ray diffraction experiment.[17,18] The theoretical curve is convoluted with the experimental resolution function as discussed in Appendix B. This convolution not only makes small wiggles appear at the bottom of the curves but also lowers and widens the peaks. The figure shows that the calculation reproduces essentially every feature in the experiment. Our calculation gives slightly better resolution than the experiment, which is perhaps surprising, as the theory includes truncation ripples via the convolution in Eq. (B9) and using the experimental $q_{\max}$.[18] What is surprising is that our simple model with no adjustable parameters even allows a quantitative comparison with experiment. This confirms that the model is adequate to be used for semiconductor alloys.

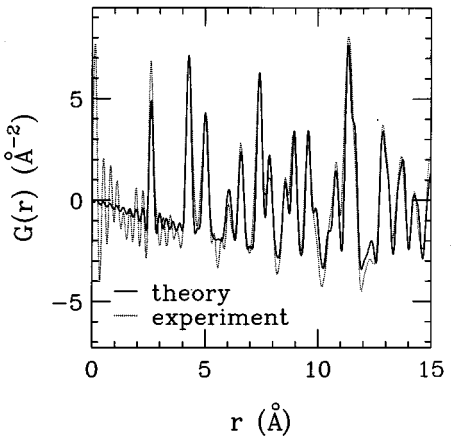

FIG. 3. The reduced (x-ray) RDF of a pure InAs crystal from the theoretical calculation (solid line) is compared with the experiment (Ref. 18) (dotted line) at 300 K.

B. Disordered system

Consider a pseudobinary semiconductor alloy in the zinc-blende structure, $A_{1-x}B_xC$ with A and B atoms in one sublattice and C in the other. Although disorder is introduced only in one sublattice in this study, it would be straightforward to generalize it to both sublattices. As mentioned before, there are two reasons for peak broadening, because the *internal strain* due to bond-length mismatch between A-C and B-C bonds comes into play as well as the *thermal motion.* As in the case of the pure crystal, for simplicity, we take $\alpha_{ij}=\alpha$ for all pairs and $\beta_{ijl}=\beta$ for all angles. We believe that this simplification does not affect the result much because the values of α and β do not vary much among III-V and II-VI compounds.[6] This restriction can easily be relaxed to include more general cases. Note that even large changes in the force constants produce only small changes in the internal strains.[5–8]

To realize the alloy, we employ the periodic supercell, which consists of $L\times L\times L$ cubic unit cells of the zinc-blende structure, each containing eight atoms. The dynamical matrix becomes a $3p\times 3p$ matrix where $p=8L^3$. This method has several advantages over other methods of calculating σ, such as the equation of motion technique.[19] Since this method simply extends the size of the basis, it is conceptually clear and we can closely follow most of the arguments about the pure system given above. Another computational merit of taking a large supercell is that we may sum only over modes at $\mathbf{k}=0$ in Eq. (18). This is because the zone folding in the reduced-zone scheme enables us to sample enough k points in the original Brillouin zone if we use a big enough supercell. It also reduces computational time since all calculations can be done in real mode rather than in complex mode. For the results presented in this section, we used $L=4$ so that we dealt with 512 atoms and hence a 1536×1536 dynamical matrix. The typical error in σ is estimated to be less than 1% by comparison with the Brillouin zone integration scheme for the perfect crystal. A configurational average is taken over 10 realizations.

The displacement vector $\mathbf{u}$ in this case contains the distortion due to the *static strain* $\mathbf{u}_s$ as well as the *thermal motion* $\mathbf{u}_t$. Since we are interested in the first-order correction in the harmonic approximation, the total $\mathbf{u}$ can be written as a simple sum of these two terms. The static strains $\mathbf{u}_s$ due to the bond-length mismatch are found by relaxing the system according to Eq. (6). The thermal fluctuations $\mathbf{u}_t$ around the relaxed positions enter through Eq. (17). The calculational procedure for alloys is as follows: for a given random number seed a configuration of the system is realized. Then the matrix $\mathbf{M}$ in Eq. (4) is constructed and the system is relaxed using the conjugate gradient method to find the static equilibrium displacement $\mathbf{u}_s$ using Eq. (6). From $\mathbf{M}$, dynami-

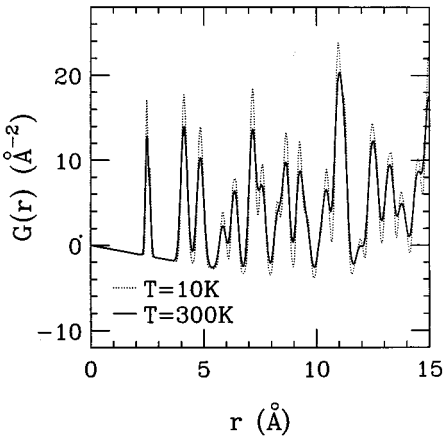

FIG. 4. Temperature variation of the reduced (neutron) RDF of a $Ga_{0.5}In_{0.5}As$ alloy is plotted as a function of the distance from the origin r at 10 K (dotted line) and 300 K (solid line). Note that the resolution does not change substantially with the temperature, and the change is much less pronounced than for the pure system shown in Fig. 2.

cal matrix **D** is numerically constructed using Eq. (7). The eigenvalue problem for the matrix **D** is solved numerically. The solution is used in the integration (18) to obtain σ_{ij}. This whole procedure is iterated over many realizations to perform a configurational average and finally Eq. (15) gives the PDF.

Figure 4 shows the reduced RDF $G(r)$ for $Ga_{0.5}In_{0.5}As$ at 10 K and 300 K. Every peak basically consists of many Gaussians as in the pure case. However, due to the internal strains each Gaussian from a particular neighbor is centered at a different distance given by the relaxed positions of each realization. The width σ_{ij} also depends on the particular realization. Therefore, we cannot make use of the symmetry of the system to reduce computational time as in the pure case. The distribution of the pair distance implies that each peak from a particular type of neighbor is already broadened even at very low temperature. Therefore, there is no dramatic change in peak width and height as in the pure system as the temperature is varied.

For comparison, the first three peaks are plotted again in Fig. 5 along with those from the pure end members, GaAs and InAs. The internal structure of the first-neighbor peak at 10 K clearly shows that it retains the characteristics of the pure systems, although this structure is almost unrecognizable at 300 K due to the thermal broadening. This is again because the nearest neighbors are only connected by the strong bond-stretching force. From the second neighbors and beyond, however, there can be many different intermediate configurations connected by the weak bond-bending forces. Hence each peak appears as a distribution of Gaussians centered at the length given by the virtual crystal approximation, with the peak of the alloy tracking the first moment of that peak, which is temperature independent and goes linearly with the composition x between the two pure crystal limits.

For a more detailed analysis, the first and the second peaks at 10 K are redrawn in Fig. 6 along with the bond-length distributions. It is clear that the structure in the first peak results from two different types of bonds (Ga-As and In-As). The lengths of two types of bonds are relaxed to new

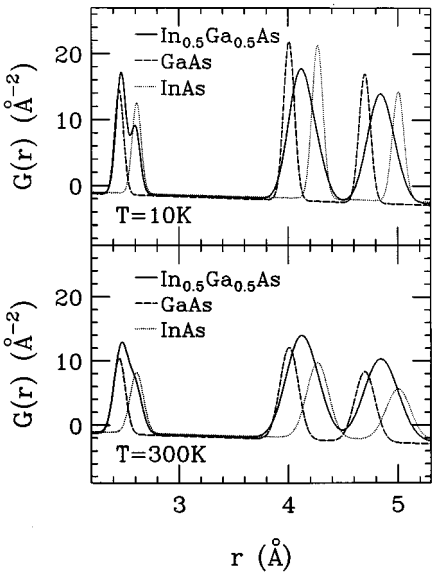

FIG. 5. Details of the first three peaks of the reduced (neutron) RDF of $Ga_{0.5}In_{0.5}As$, shown in Fig. 4, are compared with the pure end members, GaAs and InAs, at 10 K and 300 K. Solid lines are for the alloy, broken lines for GaAs, and dotted lines for InAs.

equilibrium lengths (2.47 and 2.60 Å) from those of pure cases (2.45 and 2.62 Å). This change in the bond lengths has been studied both experimentally[9] and theoretically.[6,20] Our calculation shows that the change in the average length and the width of the distribution of the nearest-neighbor bond lengths can be measured in a PDF experiment at a sufficiently low temperature. A quantitative measurement of the width may not be trivial because the thermal broadening is comparable to the width of the length distribution itself. However, it is this capability of measuring the width that

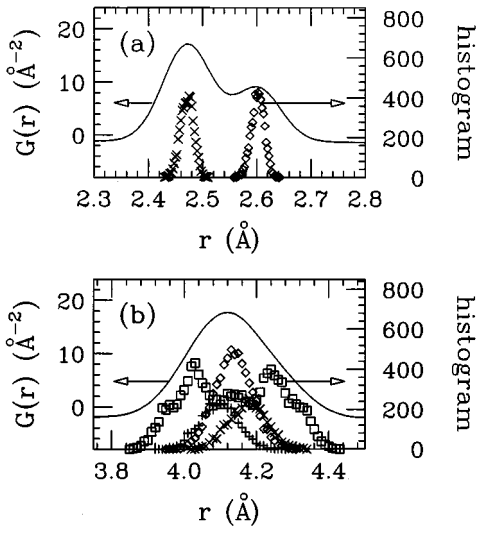

FIG. 6. Detail structures of (a) the first and (b) the second peaks of the reduced (neutron) RDF at 10 K, from Fig, 5, are drawn as solid lines to the scale in the left. The histograms of the bond-length distribution without thermal broadening are also shown to the scale in the right. In (a), × and ◇ represent Ga-As and In-As bonds, respectively. In (b), +, ×, ◇, and □ denote Ga-Ga, In-In, Ga-In, and As-As, respectively.

makes a PDF analysis potentially superior to other experimental methods. For example, XAFS experiments only measure the average length of nearest and perhaps also next-nearest-neighbor peaks. By contrast, a PDF experiment can give the average length *and* the width of the length distribution without any adjustable parameters. The only empirical parameters in our theoretical analysis are the force constants α, β and the lattice constant [See Eq. (3)]. These can be determined independently by standard experiments such as elasticity measurements and the Bragg x-ray experiment.

In the second-neighbor peak, there are four possible configurations, Ga-Ga, In-In, Ga-In from the disordered sublattice and As-As from the ordered sublattice. While the first three have only the As atom as the intermediate atom, the As-As bond can have Ga or In in the middle. Each of these five configurations has a different average length with different length distributions.[6] The length distribution can be well approximated by three Gaussians depending on environments.[20] From the bottom panel of Fig. 6, the internal structure can be seen for As-As neighbors. For others it is not discernible because the peaks from different environments are too close. In the total PDF the difference in average lengths from different configurations is within the range of thermal broadening. Therefore, the second-neighbor PDF peak appears to be a single peak at the distance given by the virtual crystal approximation and different types of neighbors are indiscernible in the total PDF.

V. CONCLUSION

In conclusion, we have developed a method of calculating the PDF of binary semiconductor crystals and pseudobinary alloys having the zinc-blende structure. The PDF reveals the local structure directly and can be compared with experiments. Our approach can be easily generalized for various crystal structures including fcc, diamond, and wurtzite structures. To facilitate the calculation, we have used a harmonic Kirkwood potential model with bond-stretching and bond-bending forces. Temperature dependence is treated quantum mechanically using the dynamical matrix and appropriate Bose factors.

The PDF turns out to consist of a series of Gaussians with weight w_{ij} given by the type of atoms at site i and j and with width σ_{ij} given as a function of phonon properties. In the case of a pure system, each type of neighbor pair has the same width and are further weighted by the number of neighbors of that type. However, in the case of the alloy, each peak from the same type of neighbor is relaxed to a different distance with a different width by the internal strains.

This method is used to calculate the PDF of a InAs pure crystal and a $Ga_{1-x}In_xAs$ alloy, with $x=0.5$. The result for the pure crystal agrees well with the diffraction experiment even though there are no adjustable parameters. The harmonic model we used describes the behavior of the system well. The result for the alloy suggests that two different types of nearest neighbors can be resolved experimentally at sufficiently low temperature. The information on the width of the length distribution can be obtained as well as the average length. The resolution of such an experiment, however, is somewhat limited by the zero point motions.

This method does not suffer from possible artifacts that may arise from fitting the experimental data with adjustable parameters, which other methods such as XAFS do. However, it has some limitations in resolution due to zero-point motions. This makes it difficult to resolve different types of bonds beyond the first-neighbor peak. One possible improvement is to explore the partial PDF, which measures peaks involving a certain atom.[21] But this would require a large experimental effort, involving isotope substitution or anomalous x-ray scattering techniques.

Despite these limitations, PDF analysis (or of course the more involved single-crystal diffuse scattering) is almost the only method of studying the intermediate-range properties of semiconductor alloys. Therefore it has been important to develop a microscopic model to understand the observed behavior microscopically and provide a clear physical picture. The model and analysis used in this study has proved to be quite versatile and robust.

ACKNOWLEDGMENTS

This work was stimulated by very helpful discussions with S. J. L. Billinge, F. Mohiuddin-Jacobs, and G. DiFrancesco. Our thanks are also extended to A. R. Day, N. Mousseau, and R. J. Elliott. This work was supported by the National Science Foundation under Grant Number CHE-92-24102. J.S.C. also acknowledges the support from the Basic Science Research Institute Program (BSRI-96-2436), Korean Ministry of Education, and from the KOSEF through a grant to the Center for Theoretical Physics, Seoul National University, Korea.

APPENDIX A: DERIVATION OF GAUSSIAN PEAKS

Let us rewrite Eq. (16) as

$$\rho_{ij}(r)=\frac{1}{2\pi}\int dq e^{-iqr}C_{ij}(q), \tag{A1}$$

where $C_{ij}(q)\equiv\langle e^{iqr_{ij}}\rangle$. In the harmonic approximation, the interatomic spacing r_{ij} can be written as

$$r_{ij}=r_{ij}^0+\mathbf{u}_{ij}\cdot\hat{r}_{ij}, \tag{A2}$$

where r_{ij}^0 is the distance between the atoms i and j in the perfect unstrained lattice. Using the Debye-Waller theorem, we have

$$C_{ij}(q)=e^{iqr_{ij}^0}\langle e^{iq\mathbf{u}_{ij}\cdot\hat{r}_{ij}}\rangle=e^{iqr_{ij}^0}e^{-(1/2)\,q^2\langle(\mathbf{u}_{ij}\cdot\hat{r}_{ij})^2\rangle}. \tag{A3}$$

Putting this back to Eq. (A1), we have

$$\rho_{ij}(r)=\frac{1}{2\pi}\int_{-\infty}^{\infty}e^{-(1/2)q^2\langle[\mathbf{u}_{ij}\cdot\hat{r}_{ij}]^2\rangle+iq(r_{ij}^0-r)}dq$$

$$=\frac{1}{\sqrt{2\pi\langle[\mathbf{u}_{ij}\cdot\hat{r}_{ij}]^2\rangle}}e^{-(r_{ij}^0-r)^2/2\langle[\mathbf{u}_{ij}\cdot\hat{r}_{ij}]^2\rangle}. \tag{A4}$$

Therefore, $\rho_{ij}(r)$ is a Gaussian peak centered at r_{ij} with the width

$$\sigma_{ij}=\langle[\mathbf{u}_{ij}\cdot\hat{r}_{ij}]^2\rangle^{1/2}, \tag{A5}$$

which is Eq. (17).

To evaluate σ_{ij}, let us divide N atoms into $\mathcal{N}$ Bravais lattice points, each containing p basis atoms as before, as described in the text. Let l (m) and μ (ν) be the unit cell label and the basis label in the unit cell of atoms i (j), respectively. Using phonon operators, the αth Cartesian component of the displacement vector $\mathbf{u}_i$ can be written as

$$u_{i\alpha}=\frac{1}{\sqrt{\mathcal{N}}}\sum_{\mathbf{k}s}\sqrt{\frac{\hbar}{2M_i\omega_s(\mathbf{k})}}[e_{\mu\alpha}(\mathbf{k}s)a_{\mathbf{k}s}e^{i\{\mathbf{k}\cdot\mathbf{r}_i-\omega_s(\mathbf{k})t\}} + e_{\mu\alpha}(-\mathbf{k}s)a^{\dagger}_{-\mathbf{k}s}e^{-i\{\mathbf{k}\cdot\mathbf{r}_i-\omega_s(\mathbf{k})t\}}] \tag{A6}$$

where $\omega_s(\mathbf{k})$ is the eigenvalue of the dynamical matrix (7) with the wave vector $\mathbf{k}$ in branch s, $e_{\mu\alpha}(\mathbf{k},s)$ is the αth component of the corresponding eigenvector associated with the atom i (basis label μ) with the mass M_μ, and $a_{\mathbf{k}s}$ ($a^{\dagger}_{\mathbf{k}s}$) is the annihilation (creation) operator. In the summation, $\mathbf{k}$ runs from 1 to $\mathcal{N}$ and s runs from 1 to $3p$. Putting this expression into Eq. (A5) and working out the commutation relations of the operators yields

$$\sigma^2_{ij}=\frac{2\hbar}{N}\sum_{\mathbf{k},s}\frac{1}{\omega_s(\mathbf{k})}\left(\langle n_{\mathbf{k},s}\rangle+\frac{1}{2}\right)\left[\frac{1}{2}\left\{\frac{|e_\mu(\mathbf{k},s)\cdot\hat{r}_{ij}|^2}{M_\mu}+\frac{|e_\nu(\mathbf{k},s)\cdot\hat{r}_{ij}|^2}{M_\nu}\right\}-\frac{|e_\mu(\mathbf{k},s)\cdot\hat{r}_{ij}||e_\nu(-\mathbf{k},s)\cdot\hat{r}_{ij}|e^{i\mathbf{k}\cdot\mathbf{r}_{ij}}}{\sqrt{M_\mu M_\nu}}\right], \tag{A7}$$

where $n_{\mathbf{k},s}$ is the number operator. This establishes Eq. (18).

APPENDIX B: MODELING FINITE DATA

In experiments, data can be collected only over a finite range of the scattering momentum q from 0 to $q_{\max}$, although the Fourier transformation in Eq. (12) should be carried out over a range from 0 to ∞. We are interested in how the termination affects the reduced RDF. In fact, the derivation in this appendix may be applied in a broader context of modeling finite data.

Let us first define a function $t(r)$ as

$$t(r)=\frac{1}{\sqrt{2\pi}}\int_0^\infty T(q)\sin qr\,dq. \tag{B1}$$

The function $T(q)$ and be any function provided that it is odd. Expanding $\sin qr$ as $(e^{iqr}-e^{-iqr})/2i$, we have

$$t(r)=\frac{1}{\sqrt{2\pi}}\frac{1}{2i}\left[\int_0^\infty T(q)e^{iqr}dq+\int_0^{-\infty}T(-q)e^{iqr}dq\right], \tag{B2}$$

where we have made a change in variable, $q\to -q$, in the second integral. Combining the integrals and noting that $T(-q)=-T(q)$, we get

$$t(r)=\frac{1}{\sqrt{2\pi}}\int_{-\infty}^{\infty}\frac{T(q)}{2i}e^{iqr}dq, \tag{B3}$$

and thus, through a back Fourier transform,

$$\frac{T(q)}{2i}=\frac{1}{\sqrt{2\pi}}\int_{-\infty}^{\infty}t(r)e^{-iqr}dr, \tag{B4}$$

Now we are interested in knowing that we will recover in real space in the case when we collect data only out to $q_{\max}$. Hence, we define

$$t'(r)=\frac{1}{\sqrt{2\pi}}\int_0^{q_{\max}}T(q)\sin qr\,dq, \tag{B5}$$

which, in analogy with Eqs. (B1) through (B3), gives

$$t'(r)=\frac{1}{\sqrt{2\pi}}\int_{-q_{\max}}^{q_{\max}}\frac{T(q)}{2i}e^{iqr}dq. \tag{B6}$$

Substituting Eq. (B4) for $T(q)/2i$ and evaluating the integral over q, we get

$$t'(r)=\frac{1}{\pi}\int_{-\infty}^{\infty}t(r')\frac{\sin q_{\max}(r-r')}{r-r'}dr'. \tag{B7}$$

Since $t(r)$ is also an odd function, we can use $t(-r)=-t(r)$ to obtain

$$t'(r)=\frac{1}{\pi}\int_0^\infty t(r')\left[\frac{\sin q_{\max}(r-r')}{r-r'}-\frac{\sin q_{\max}(r+r')}{r+r'}\right]dr'. \tag{B8}$$

We can now substitute directly $G(r)$ giving

$$G_e(r)=\frac{1}{\pi}\int_0^\infty G(r')\left[\frac{\sin q_{\max}(r-r')}{r-r'}-\frac{\sin q_{\max}(r+r')}{r+r'}\right]dr', \tag{B9}$$

where $G_e(r)$ is the experimentally determined reduced RDF from finite data. The function in the brackets makes the ideal $G(r)$ broader and produces ripples around the peak in Fig. 3.

*Permanent address: Department of Physics, Chungbuk National University, Cheongju, 360-763, Republic of Korea.

[1] V. Narayanamurti, Science **235**, 1023 (1987).
[2] L. Vegard, Z. Phys. **5**, 17 (1921).
[3] L. Nordheim, Ann. Phys. (Leipz.) **9**, 607 (1931); **9**, 641 (1931).
[4] M. F. Thorpe, W. Jin, and S. D. Mahanti, in *Disorder in Condensed Matter Physics*, edited by by J. A. Blackman and J. Taguena (Oxford University Press, New York, 1991), p. 22.
[5] Y. Cai and M. F. Thorpe, Phys. Rev. B **46**, 15 872 (1992).
[6] Y. Cai and M. F. Thorpe, Phys. Rev. B **46**, 15 879 (1992).
[7] N. Mousseau and M. F. Thorpe, Phys. Rev. B **46**, 15 887 (1992).
[8] R. W. Wang, M. F. Thorpe, and N. Mousseau, Phys. Rev. B **52**, 17 191 (1992).
[9] J. C. Mikkelsen, Jr. and J. B. Boyce, Phys. Rev. Lett. **49**, 1412 (1982); Phys. Rev. B **28**, 7130 (1983).
[10] B. E. Warren, *X-ray Diffraction* (Addison-Wesley, Reading, 1969).
[11] G. S. Cargill III, in *Solid State Physics*, Vol. 30, edited by H. Ehrenreich, F. Seitz, and D. Turnbull (Academic Press, New York, 1975).
[12] S. R. Elliott, *Physics of Amorphous Materials* (Longman Scientific & Technical, London, 1990).

[13] T. Egami, Mater. Trans. **31**, 163 (1990).
[14] Different nomenclatures have been used in literature. See Sec. III for definitions. To minimize confusion we use conventional notations such as $\rho(r)$ for PDF and $G(r)$ for reduced RDF.
[15] J. G. Kirkwood, J. Chem. Phys. **7**, 506 (1939).
[16] P. N. Keating, Phys. Rev. **145**, 637 (1966).
[17] A. A. Maradudin, E. W. Montroll, G. H. Weiss, and I. P. Ipatova, *Theory of Lattice Dynamics in the Harmonic Approximation* (Academic Press, New York, 1971).
[18] F. Mohiuddin-Jacob and S. J. L. Billinge (private communication); Bull. Am. Phys. Soc. **41**, 592 (1996).
[19] M. F. Thorpe and S. W. de Leeuw, Phys. Rev. B **33**, 8490 (1986).
[20] M. C. Schabel and J. L. Martins, Phys. Rev. B **43**, 11 873 (1991).
[21] S. J. L. Billinge (private communication).